International Journal of Computational Methods
Vol. 14, No. 1 (2017) 1750020 (19 pages)
© World Scientific Publishing Company
DOI: 10.1142/S0219876217500207

World Scientific
www.worldscientific.com

Numerical Simulations Using TVD Schemes of Two-Dimensional Supersonic Flow in Chemical Equilibrium

J. Saldía* and S. Elaskar†

Department of Aeronautics
National University of Córdoba
Institute for Advanced Studies in Engineering
and Technology (IDIT-CONICET), Córdoba, Argentina
**jsaldia@conicet.gov.ar*
†*selaskar@unc.edu.ar*

J. Tamagno

Department of Aeronautics
National University of Córdoba
Córdoba, Argentina
jtamagno@efn.uncor.edu

Received 20 April 2015
Accepted 19 June 2016
Published 1 August 2016

A numerical scheme for the solution of both unsteady and steady-state, two-dimensional Euler equations considering gas in chemical equilibrium, is presented. Three alternatives of the Total Variation Diminishing (TVD) Harten–Yee scheme are implemented. One of them is a technique based on the adaptive use of different limiter functions in each wave of the inter-cell Riemann problem. With this technique, the undesirable effects of the artificial viscosity on the capture of contact discontinuities are reduced, without loss of robustness in nonlinear waves resolution. In order to verify the accuracy of the proposed scheme, results of the unsteady flow in cylindrical explosions, and of the steady-state solution of hypersonic flow over a blunt body, are presented. Finally, comparisons considering accuracy of results and convergence properties between the three Harten–Yee schemes are carried out.

Keywords: TVD schemes; chemical equilibrium; hypersonic flows.

Int. J. Comput. Methods Downloaded from www.worldscientific.com
by NANYANG TECHNOLOGICAL UNIVERSITY on 08/06/16. For personal use only.

1. Introduction

Shocks and contact surfaces are physical discontinuities, which arise in solving Euler equations, the system that describes the dynamics of general compressible non-viscous flows [Whitham (1974)] and [Tamagno *et al.* (2003)]. The accuracy of a numerical discretization of this system, its ability to capture discontinuities and

Int. J. Comput. Methods Downloaded from www.worldscientific.com
by NANYANG TECHNOLOGICAL UNIVERSITY on 08/06/16. For personal use only.

the correct prediction of wave velocities is strongly dependent on the numerical fluxes evaluation. Second-order schemes have the ability of solving these discontinuities accurately, but they are also proclive to introduce spurious oscillations in the solution. On the other hand, first-order schemes do not introduce oscillations, but they present the disadvantage of smearing the discontinuities excessively [Toro (2009)] and [Leveque (2004)]. A class of high-order schemes known as Total Variation Diminishing (TVD) Schemes present both the advantage of solving accurately the discontinuities without introducing unphysical oscillations. However, the TVD condition has been proven only in the scalar convection equation [Harten and Hyman (1983b)]. Thus, if the TVD schemes are applied for general nonlinear equation systems, the numerical solutions may not be oscillations free. When applying the TVD scheme originally devised by [Harten and Hyman (1983b)] and later modified by [Yee (1986); Yee (1987a)], (at present called Harten–Yee TVD scheme), to numerically solve Euler equations, the discontinuities associated to linearly degenerated waves family are very hard of solving accurately, unless highly compressive limiter functions are used. However, compressive limiter functions present certain disadvantages: lack of robustness in the capture of shock waves, nonfree unphysical oscillatory solutions, poor convergence rates and poor numerical stability in 2D and 3D steady-state calculations [Zheng and Lee (1998)].

In more recent papers [Falcinelli *et al.* (2008)] and [Elaskar *et al.* (2009)], an adaptive use of limiter functions in the context of the Harten–Yee TVD scheme for calorically perfect gas was proposed. In this technique, if under a comparison criteria, the strengths of the linearly degenerate waves family are higher than the strength of the genuinely nonlinear waves family, then a highly compressive limiter function, know as *superbee*, is applied to the linearly degenerate wave family. Otherwise, the original upwind scheme of Yee, which uses the more diffusive *minmod* limiter function in all waves, is employed. This scheme has shown ability in solving accurately contact discontinuities without losing robustness in capturing shock waves. In a previous paper, the one-dimensional supersonic flow in chemical equilibrium using an adaptive scheme for the limiter functions [Saldia *et al.* (2015)] was studied. Now, the main objective of this work is to extend this technique to solve two-dimensional, time-dependent and steady-state Euler equations, considering a working gas in thermo-chemical equilibrium. Results obtained solving Riemann problems with cylindrical symmetry specifically selected to enhance the differences between thermo-chemical equilibrium states, and its perfect caloric counterpart [Vinokur (1989)] and [Vinokur and Montagné (1990)], and from solving steady-state hypersonic flows over a blunt body, are presented and discussed.

2. Governing Equations

The Euler equations form a nonlinear hyperbolic system of differential equations, that describe the dynamics of a compressible gas flow disregarding the effects of mass forces, viscosity and heat transfer by conduction and radiation. The unsteady

two-dimensional Euler equations defined on a Cartesian coordinate system (x, y) can be written in conservation form as:

$$\frac{\partial \mathbf{u}}{\partial t} + \frac{\partial \mathbf{f}(\mathbf{u})}{\partial x} + \frac{\partial \mathbf{g}(\mathbf{u})}{\partial y} = \mathbf{0}, \tag{1}$$

where t denotes the temporal variable and where $\mathbf{u}$, the vector of conservative variables, is

$$\mathbf{u}^T = [\rho, \rho \mathsf{v}_x, \rho \mathsf{v}_y, E]. \tag{2}$$

The inviscid fluxes are written as

$$\begin{aligned} \mathbf{f}^T &= [\rho \mathsf{v}_x, \rho \mathsf{v}_x^2 + p, \rho \mathsf{v}_x \mathsf{v}_y, \mathsf{v}_x(E + p)], \\ \mathbf{g}^T &= [\rho \mathsf{v}_y, \rho \mathsf{v}_x \mathsf{v}_y, \rho \mathsf{v}_y^2 + p, \mathsf{v}_y(E + p)], \end{aligned} \tag{3}$$

where ρ is the density, v_x and v_y are the velocity components, p is the pressure, and the total energy is given by

$$E = \rho \left(e + \frac{1}{2}(\mathsf{v}_x^2 + \mathsf{v}_y^2) \right). \tag{4}$$

In this work, the closure of the Euler equations systems is provided by solving the chemical equilibrium state of the fluid at a given density ρ and specific internal energy e, assuming that the fluid is a mixture of thermally perfect gases, that obeys the equation of state

$$p = \rho \frac{R}{W} T, \tag{5}$$

where R is the universal gas constant, T is the thermodynamic temperature and W is the molecular mass of the gas mixture given by the chemical equilibrium composition.

3. Numerical Scheme

In this paper, to solve the Euler equations, a two-dimensional finite difference method has been used. Moreover, to evaluate the numerical fluxes, an extension of the Harten–Yee TVD scheme, which uses an adaptive method of different limiter functions for each wave of the Riemann problem, has been implemented.

3.1. *Spatial discretization*

To implement the Harten–Yee scheme, a coordinate transformation between the physical domain and the computational domain has been utilized. Let (x, y) and (ξ, η) be the system of coordinates that represent the physical and computational domains, respectively, and $\xi = \xi(x, y)$ and $\eta = \eta(x, y)$ the mapping between both.

Int. J. Comput. Methods Downloaded from www.worldscientific.com
by NANYANG TECHNOLOGICAL UNIVERSITY on 08/06/16. For personal use only.

Int. J. Comput. Methods Downloaded from www.worldscientific.com
by NANYANG TECHNOLOGICAL UNIVERSITY on 08/06/16. For personal use only.

The system (1) can be written in terms of computational domain coordinates through,

$$\frac{\partial \hat{\mathbf{u}}}{\partial t} + \frac{\partial \hat{\mathbf{f}}(\hat{\mathbf{u}})}{\partial \xi} + \frac{\partial \hat{\mathbf{g}}(\hat{\mathbf{u}})}{\partial \eta} = \mathbf{0}, \tag{6a}$$

where,

$$\hat{\mathbf{u}} = \mathbf{u}/J, \tag{6b}$$

$$\hat{\mathbf{f}} = (\xi_x \mathbf{f} + \xi_y \mathbf{g})/J, \tag{6c}$$

$$\hat{\mathbf{g}} = (\eta_x \mathbf{f} + \eta_y \mathbf{g})/J \tag{6d}$$

and J is the Jacobian of the coordinate transformation given by:

$$J = \xi_x \eta_y - \xi_y \eta_x. \tag{6e}$$

Let $(\xi_i, \eta_j) = (i\Delta\xi, j\Delta\eta)$ denote the nodes coordinates defined on the computational grid. Let $\hat{\mathbf{u}}_{i,j} = \mathbf{u}(\xi_i, \eta_j)/J_{i,j}$ be the vector of conservative variables transformed to the computational grid, where $J_{i,j}$ is the Jacobian of the coordinate transformation for the point (i, j). Therefore, a discretized conservative form of system (6a) can be written as:

$$\frac{\partial \hat{\mathbf{u}}_{i,j}}{\partial t} = -\frac{1}{\Delta\xi}(\tilde{\mathbf{f}}_{i+\frac{1}{2},j} - \tilde{\mathbf{f}}_{i-\frac{1}{2},j}) - \frac{1}{\Delta\eta}(\tilde{\mathbf{g}}_{i,j+\frac{1}{2}} - \tilde{\mathbf{g}}_{i,j-\frac{1}{2}}). \tag{7}$$

For the Harten–Yee scheme, the numerical flux $\tilde{\mathbf{f}}_{i+\frac{1}{2},j}$ can be defined as [Yee (1987)],

$$\tilde{\mathbf{f}}_{i+\frac{1}{2},j} = \left[\left(\frac{\xi_x}{J}\right)_{i+\frac{1}{2},j}(\mathbf{f}_{i,j} + \mathbf{f}_{i+1,j}) + \left(\frac{\xi_y}{J}\right)_{i+\frac{1}{2},j}(\mathbf{g}_{i,j} + \mathbf{g}_{i+1,j})\right] + \frac{1}{2}(\mathbf{R}_\xi)_{i+\frac{1}{2},j}\,\boldsymbol{\Phi}_{i+\frac{1}{2},j} \Big/ J_{i+\frac{1}{2},j}, \tag{8}$$

where $\mathbf{f}_{i,j}$ denotes $\mathbf{f}(\mathbf{u}_{i,j})$. In this paper, the derivatives of the coordinates transformation ξ_x, ξ_y and the Jacobians $J_{i+\frac{1}{2},j}$ are calculated according to [Yee (1989)]:

$$\left(\frac{\xi_x}{J}\right)_{i+\frac{1}{2},j} = \frac{1}{2}\left[\left(\frac{\xi_x}{J}\right)_{i,j} + \left(\frac{\xi_x}{J}\right)_{i+1,j}\right], \tag{9a}$$

$$\frac{1}{J_{i+\frac{1}{2},j}} = \frac{1}{2}\left(\frac{1}{J_{i,j}} + \frac{1}{J_{i+1,j}}\right). \tag{9b}$$

The matrix $(\mathbf{R}_\xi)_{i+\frac{1}{2},j}$ in (8) is a matrix, whose columns corresponds to the right eigenvectors of the Jacobian matrix $\hat{\mathbf{A}} = \xi_x \frac{\partial \mathbf{f}}{\partial \mathbf{u}} + \xi_y \frac{\partial \mathbf{g}}{\partial \mathbf{u}}$ evaluated at the generalized Roe's average state [Vinokur and Montagné (1990)].

The l-components of the numerical dissipation vector $\boldsymbol{\Phi}_{i+\frac{1}{2}}$ are given by

$$\Phi^l_{i+\frac{1}{2}} = \frac{1}{2}\psi(\lambda^l_{i+\frac{1}{2}})(g^l_i + g^l_{i+1}) - \psi\left(\lambda^l_{i+\frac{1}{2}} + \gamma^l_{i+\frac{1}{2}}\right)\alpha^l_{i+\frac{1}{2}}, \tag{10}$$

where for simplicity reasons we avoid the suffix j hereafter.

Int. J. Comput. Methods Downloaded from www.worldscientific.com
by NANYANG TECHNOLOGICAL UNIVERSITY on 08/06/16. For personal use only.

Moreover, $\alpha^l_{i+\frac{1}{2}}$ are the components of the spectral decomposition vector of the Riemann problem at cell interfaces:

$$\boldsymbol{\alpha} = (\mathbf{R}^{-1}_{\xi})_{i+\frac{1}{2}}(\mathbf{u}_{i+1} - \mathbf{u}_i) = \begin{bmatrix} \frac{1}{2}(aa + bb + \Delta_{i+\frac{1}{2}}\rho) \\ -aa \\ cc \\ \frac{1}{2}(aa - bb + \Delta_{i+\frac{1}{2}}\rho) \end{bmatrix}, \tag{11a}$$

$$aa = \frac{\tilde{\kappa}}{\tilde{c}^2}\left[\Delta_{i+\frac{1}{2}}E - (\hat{H} - \tilde{\mathsf{v}}_x^2 - \tilde{\mathsf{v}}_y^2)\Delta_{i+\frac{1}{2}}\rho - \tilde{\mathsf{v}}_x\Delta_{i+\frac{1}{2}}\rho\mathsf{v}_x - \tilde{\mathsf{v}}_y\Delta_{i+\frac{1}{2}}\rho\mathsf{v}_y\right], \tag{11b}$$

$$bb = \frac{1}{\tilde{c}}\left[-(k_1)_{i+\frac{1}{2}}\Delta_{i+\frac{1}{2}}\rho\mathsf{v}_x - (k_2)_{i+\frac{1}{2}}\Delta_{i+\frac{1}{2}}\rho\mathsf{v}_y + \left((k_1)_{i+\frac{1}{2}}\tilde{\mathsf{v}}_x + (k_2)_{i+\frac{1}{2}}\tilde{\mathsf{v}}_y\right)\Delta_{i+\frac{1}{2}}\rho\right], \tag{11c}$$

$$cc = (k_1)_{i+\frac{1}{2}}\Delta_{i+\frac{1}{2}}\rho\mathsf{v}_y - (k_2)_{i+\frac{1}{2}}\Delta_{i+\frac{1}{2}}\rho\mathsf{v}_x + \left((k_2)_{i+\frac{1}{2}}\tilde{\mathsf{v}}_x - (k_1)_{i+\frac{1}{2}}\tilde{\mathsf{v}}_y\right)\Delta_{i+\frac{1}{2}}\rho, \tag{11d}$$

where $\Delta_{i+\frac{1}{2}}() \equiv ()_{i+1} - ()_i$, and where the upper tilde denotes the average state of Roe between the states $\mathbf{u}_{i+1}$ and $\mathbf{u}_i$. The geometric coefficients are

$$(k_1)_{i+\frac{1}{2}} = \frac{\left(\frac{\xi_x}{J}\right)_{i+\frac{1}{2}}}{\sqrt{\left(\frac{\xi_x}{J}\right)^2_{i+\frac{1}{2}} + \left(\frac{\xi_y}{J}\right)^2_{i+\frac{1}{2}}}} \tag{12}$$

with an analogous definition for $(k_2)_{i+\frac{1}{2}}$.

$\lambda^l_{i+\frac{1}{2}}$ in (10), denotes the l-eigenvalue of the Jacobian matrix $\hat{\mathbf{A}}$, and $\gamma^l_{i+\frac{1}{2}}$ is the term that modifies the characteristic speed value and it is given by:

$$\gamma^l_{i+\frac{1}{2}} = \begin{cases} (g^l_{i+1} - g^l_i)/\Delta_{i+\frac{1}{2}}u^l, & \text{if } \Delta_{i+\frac{1}{2}}u^l \neq 0, \\ 0, & \text{if } \Delta_{j+\frac{1}{2}}u^l = 0, \end{cases} \tag{13}$$

where u^l is the l-component of the vector of conservative variables $\mathbf{u}$. The function $\psi(z)$, also known as "entropy fix", is necessary to guarantee the scheme convergence toward the physically relevant solution. It is given by [Harten (1983a)]:

$$\psi(z) = \begin{cases} |z|, & \text{if } |z| \geq \epsilon, \\ (z^2 + \epsilon^2)/2\epsilon, & \text{if } |z| < \epsilon, \end{cases} \tag{14}$$

where ϵ is a small parameter, that can be either constant or solution dependent.

The scalar function g^l_i is the flux limiter function and is closely related to the TVD property of the scheme. In the selection of limiter functions, the methodology proposed by [Falcinelli *et al.* (2008)] and [Elaskar *et al.* (2009)] is used. In this technique, the superscript l in (10) is considered to be associated either to a linearly degenerated family or to a genuinely nonlinear family of characteristic waves of the

Int. J. Comput. Methods Downloaded from www.worldscientific.com
by NANYANG TECHNOLOGICAL UNIVERSITY on 08/06/16. For personal use only.

hyperbolic system of equations. Then, the strength of the spectral decomposition vector components are compared under a certain imposed criteria. If the strength of those components associated to the linearly degenerated family are higher than the corresponding to genuinely nonlinear family waves, the *superbee* [Ro (1986)] limiter function is employed with all $l's$ associated to the linearly degenerated family, and the *minmod* limiter function [Harten and Hyman (1983b)] with the rest. Otherwise, only the *minmod* limiter is used with all waves. This way of proceeding aims to take advantage of what each limiter function does better, that is, getting robustness without introducing oscillations with the *minmod* function, and high resolutions in contact discontinuities with the *superbee* function.

The aforementioned *minmod* limiter is given by:

$$g_i^l = \text{minmod}(\Delta_{i-1/2}(u^l), \Delta_{i+1/2}(u^l)) \tag{15}$$

and the minmod function takes the smaller absolute value of its arguments, if these are of the same sign, and zero otherwise. The *superbee* limiter function [Ro (1986)] is defined as:

$$g_i^l = S \cdot \max\left[0, \min\left(2\left|\alpha^l_{i+\frac{1}{2}}\right|, S \cdot \alpha^l_{i-\frac{1}{2}}\right), \min\left(\left|\alpha^l_{i+\frac{1}{2}}\right|, 2S \cdot \alpha^l_{i-\frac{1}{2}}\right)\right];$$

$$S = \text{sign}(\Delta_{i+\frac{1}{2}} u^l). \tag{16}$$

The adaptive technique for selecting the limiter function is defined by performing the following steps: first, the eigenvalues of the Jacobian matrix $\hat{\mathbf{A}}$ are numbered according to

$$\lambda^{(1,4)} = \xi_x \mathsf{v}_x + \xi_y \mathsf{v}_y \mp \sqrt{\xi_x^2 + \xi_y^2}\, c,$$

$$\lambda^{(2,3)} = \xi_x \mathsf{v}_x + \xi_y \mathsf{v}_y.$$

With this definition, the $l = 1, 4$-characteristic waves correspond to genuinely nonlinear fields and the $l = 2, 3$-characteristic waves to linearly degenerate fields. Then, the l-characteristic waves intensity I^l operator is defined

$$I^l = \|\alpha^l_{i+\frac{1}{2}} (\mathbf{R}_\xi)^l_{i+\frac{1}{2}}\|. \tag{17}$$

Finally, the rule for selecting limiter functions can be expressed as follows:

$$\begin{cases} \text{minmod in all waves} & \text{if } \max\,(I^{(2)}, I^{(3)}) \le \max\,(I^{(1)}, I^{(4)}), \\ \text{superbee in waves 2 and 3} & \text{if } \max\,(I^{(2)}, I^{(3)}) > \max(I^{(1)}, I^{(4)}). \end{cases} \tag{18}$$

3.2. *Time integration*

The time integration is carried out through an explicit Runge–Kutta like scheme developed by [Gottlieb and Shu (1998)], which was specifically designed with the aim of preserving the TVD property of the spatial discretization. Also, this Runge–Kutta method reduces high frequency numerical oscillations, therefore, is also suitable for steady-state simulations. Let us call $L(\mathbf{u})$ the right-hand side operator of (7); then,

the implemented second-order Runge–Kutta method can be written as [Gottlieb and Shu (1998)]:

$$\hat{\mathbf{u}}_{i,j}^{(1)} = \hat{\mathbf{u}}_{i,j}^{n} + \Delta t L(\hat{\mathbf{u}}^{n}), \tag{19a}$$

$$\hat{\mathbf{u}}_{i,j}^{n+1} = \frac{1}{2}\hat{\mathbf{u}}_{i,j}^{n} + \frac{1}{2}\hat{\mathbf{u}}_{i,j}^{(1)} + \frac{1}{2}\Delta t L(\hat{\mathbf{u}}^{(1)}), \tag{19b}$$

where the CFL condition is given by $\Delta t \leq \min_{i,j}\{\min(\frac{\Delta\xi}{|\mathrm{v}_\xi|+c}, \frac{\Delta\eta}{|\mathrm{v}_\eta|+c})_{i,j}\}$, in which c denotes the speed of sound.

Int. J. Comput. Methods Downloaded from www.worldscientific.com
by NANYANG TECHNOLOGICAL UNIVERSITY on 08/06/16. For personal use only.

3.3. *Chemical equilibrium calculations*

To compute the thermodynamic properties of the chemical equilibrium gas mixture, the CEA program (*Chemical Equilibrium with Applications*) [Gordon and McBride (1994)], developed by NASA-Glenn Research Center is employed. However, for efficiency purposes, a database, that stores discrete values of required thermodynamical variables in the numerical scheme has been built. Then, an efficient interpolation procedure of these values is used during the fluid flow computations. This procedure has increased the accuracy without incurring in an additional computational cost, in comparison with another widely used approach, the Tannehill curves fit, in spite of the fact that the latter is only valid for air [Tannehill and Mugge (1974)].

The database is stored in a matrix, called here $\mathcal{C}^{\mathrm{SET}}$, whose elements $c_{i,j}^{\mathrm{SET}}$ store information about pressure, internal energy, temperature and thermodynamic derivatives. To obtain thermodynamics variables from the matrix elements, the input variables are the density and the internal energy, because these variables are obtained directly from the conservative state vector of Euler equations.

To evaluate the corresponding chemical equilibrium thermodynamic properties at a given density and internal energy, an interpolating procedure has been implemented. It takes advantage of the physical fact of the internal energy is a monotonically increasing function with temperature for constant density. This interpolating procedure can be described as follows.

Given an input density ρ satisfying

$$\log(\rho_j) \leq \log(\rho) \leq \log(\rho_{j+1}), \tag{20}$$

where $\log(\rho_j)$ denotes the (constant) value of density, which corresponds to a j-column of $\mathcal{C}^{\mathrm{SET}}$, let $m_j(\rho)$ be defined as:

$$m_j(\rho) = \frac{\log(\rho) - \log(\rho_j)}{\log(\rho_{j+1}) - \log(\rho_j)}, \quad \rho_j \leq \rho \leq \rho_{j+1}. \tag{21}$$

The value of the internal energy e is known from the Euler system, and it satisfies

$$\log(e_{i_L,j}) \leq \log(e) \leq \log(e_{i_L+1,j}), \tag{22a}$$

$$\log(e_{i_R,j+1}) \leq \log(e) \leq \log(e_{i_R+1,j+1}), \tag{22b}$$

where $e_{i,j}$ are the values for the internal energy stored in the elements $c_{i,j}$ of $\mathcal{C}^{\mathrm{SET}}$. Now, let $n_L(e)$ and $n_R(e)$ be respectively defined as

$$n_L(e) = \frac{\log(e) - \log(e_{i_L,j})}{\log(e)_{i_L+1,j} - \log(e_{i_L,j})}, \quad e_{i_L,j} \leq e \leq e_{i_L+1,j}, \tag{23a}$$

$$n_R(e) = \frac{\log(e) - \log(e_{i_R,j})}{\log(e)_{i_R+1,j} - \log(e_{i_R,j})}, \quad e_{i_R,j+1} \leq e \leq e_{i_R+1,j+1}. \tag{23b}$$

Given the above definitions the interpolation procedure to compute a generic thermodynamic variable β stored in $\mathcal{C}^{\mathrm{SET}}$ is accomplished through the evaluation of

$$\beta(\rho, e) = \beta_L(e)(1 - m_j(\rho)) + \beta_R(e)m_j(\rho), \tag{24}$$

where

$$\beta_L(e) = \beta_{i_L,j}(1 - n_L(e)) + \beta_{i_L+1,j}n_L(e), \tag{25a}$$

$$\beta_R(e) = \beta_{i_R,j+1}(1 - n_R(e)) + \beta_{i_R+1,j+1}n_R(e). \tag{25b}$$

To validate this interpolation methodology, comparisons have been made with results obtained by means of both the Tannehill curves and the CEA program for air in a wide range of conditions. It was found that the interpolation procedure gives an acceptable accuracy with considerable reduction in computing times, when compared to the CEA program [Saldía (2012)].

4. Results

In this section, results from numerical tests performed with the aim of testing the behavior of the adaptive technique, when applied to both unsteady and steady two-dimensional chemical equilibrium flows computations are presented.

4.1. *Unsteady problems*

Three Riemann problems with cylindrical symmetry are presented. Note that these tests have been previously implemented by [Yee (1989)] and [Montagné *et al.* (1989)] to compare the performances of TVD schemes, when the gas is considered in chemical equilibrium. The initial conditions of the Riemann problem with cylindrical symmetry are defined with respect to the radial distance $r = \sqrt{x^2 + y^2}$ as $\mathbf{u}(x, y, t = 0) = \mathbf{u}^{(I)}$, if $r < r_c$ and $\mathbf{u}(x, y, t = 0) = \mathbf{u}^{(E)}$, if $r > r_c$, where (I) and (E) stands for internal and external states, respectively. The initial conditions of the respective test cases are shown in Table 1.

The physical domain consists in a square of length $L = 14.0\,\mathrm{m}$, $0 \leq x, y \leq L$. The cylinder radius is $r_c = 7.0\,\mathrm{m}$. A Cartesian mesh with constant mesh size of $0.14\,\mathrm{m}$ is employed (101×101 mesh points). The domain is reduced by symmetrical boundary conditions imposed on $x = 0$ and $y = 0$ sides, and exit boundary conditions on sides, where $x = L$ and $y = L$. The working gas is air (79% N_2 and 21% O_2). The chemical species considered are: N_2, O_2, NO, N, O, NO^+ and e^-. For all simulations, the

Int. J. Comput. Methods Downloaded from www.worldscientific.com
by NANYANG TECHNOLOGICAL UNIVERSITY on 08/06/16. For personal use only.

Table 1. Riemann problems with cylindrical symmetry. Initial conditions of test cases.

Test	State	Density (kg/m^3)	Pressure (Pa)	Temperature (K)
A	(I)	0.0660	9.84×10^4	4390.8
	(E)	0.030	1.50×10^4	1741.8
B	(I)	1.40	9.88×10^5	2456.5
	(E)	0.140	9.93×10^3	247.1
C	(I)	1.0	6.50×10^5	2263.6
	(E)	0.010	1.00×10^3	348.4

Int. J. Comput. Methods Downloaded from www.worldscientific.com
by NANYANG TECHNOLOGICAL UNIVERSITY on 08/06/16. For personal use only.

parameter ϵ of the entropy fix (14) is constant and equal to 0.10. Three variations of the Harten–Yee scheme are implemented: the first one, called Harten–Yee Adaptive (HYAD), is the adaptive technique already described in Sec. 3.1. The second one, here called Harten–Yee Minmod (HYMM), employs the *minmod* limiter in all waves without taking into consideration, if the characteristics fields of these waves are nonlinear or linearly degenerates. The last one, here called Harten–Yee NonAdaptive (HYNAD), employs the *minmod* limiter in the genuinely nonlinear waves and the *superbee* limiter in the linearly degenerate waves in all the domain.

Figures 1–3 plot the temperature solution with respect to the radial distance for test cases A, B and C, respectively. The numerical solutions are compared with those obtained through the solution of the one-dimensional Euler equations with cylindrical symmetry source terms on a fine mesh of 5,000 nodes (called here as "exact"). The plotted results correspond to the diagonal line given by $y = x$, because along this line, the mesh has the greatest misalignment with respect to the waves

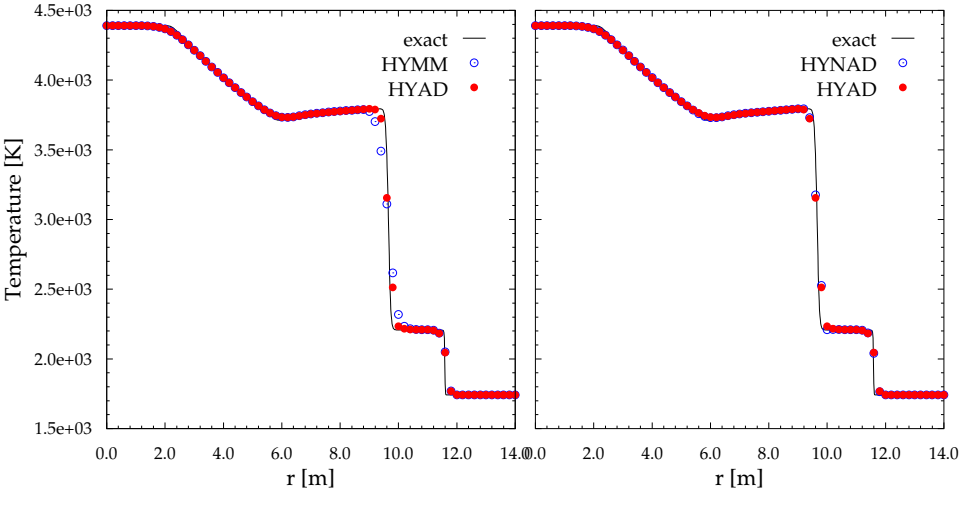

Fig. 1. Test case A. Comparison of limiter functions. Time: 3.5 ms.

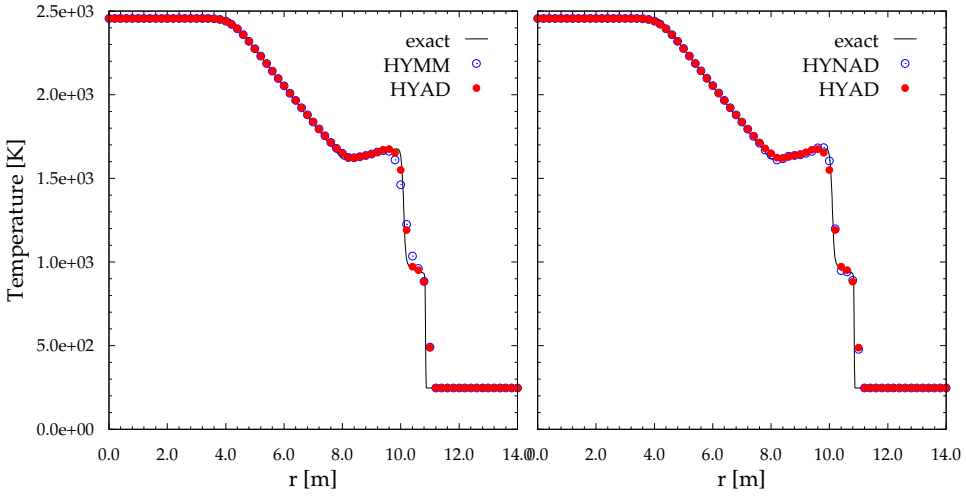

Fig. 2. Test case B. Comparison of limiter functions. Time: 3.0 ms.

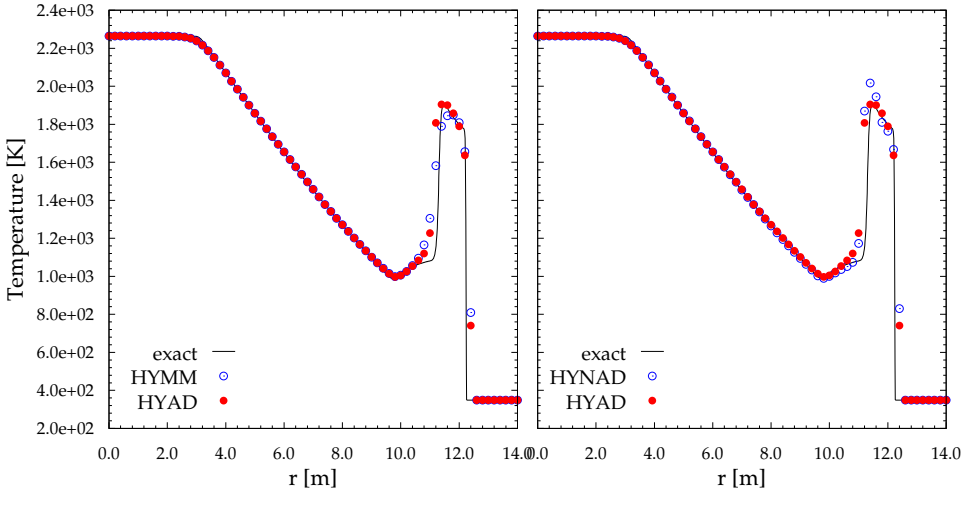

Fig. 3. Test case C. Comparison of limiter functions. Time: 3.2 ms.

propagation direction. However, the results over other radial lines showed similar accuracy.

Results obtained for test A are shown in Fig. 1. The output shown corresponds to a simulation time of $t = 3.5$ ms. The resultant wave pattern of the Riemann problem is composed of an expansion wave, which moves to the center of the cylinder and a contact wave and a shock moving in the opposite direction. From Fig. 1, it can be observed that both the schemes HYAD and HYNAD improve the contact discontinuity resolution in comparison with HYMM, and show similar accuracy

Int. J. Comput. Methods Downloaded from www.worldscientific.com
by NANYANG TECHNOLOGICAL UNIVERSITY on 08/06/16. For personal use only.

in the numerical capture of the shock wave. In this last regard, the three schemes present a similar behavior, capturing the shock wave in a total of three cells. Figure 2 shows results of temperature for the test B at time $t = 3.0\,\text{ms}$. The general wave pattern in this case is similar to the already described in test A. For this case, the three schemes capture the shock wave in two cells. The schemes which employs the *superbee* limiter function presents a similar general behavior and captures in only two cells, the contact wave while the scheme HYMM requires a total of four cells for this purpose.

Figure 3 shows the temperature solution for test C corresponding to time $t = 4.2\,\text{ms}$. The advantages of employing the adaptive scheme (HYAD) are best illustrated with this test. It can be observed that the nonadaptive application of the *superbee* limiter corresponding to scheme HYNAD produces an over estimation and oscillations near the contact surface, which are damped with the scheme HYAD. Also, the HYAD scheme solves more accurately this discontinuity wave than the traditional HYMM scheme.

4.2. *Steady hypersonic flows*

A steady-state hypersonic flow simulation over a blunt body is presented in this section. The gas considered is air and the flow is assumed to be in thermo-chemical

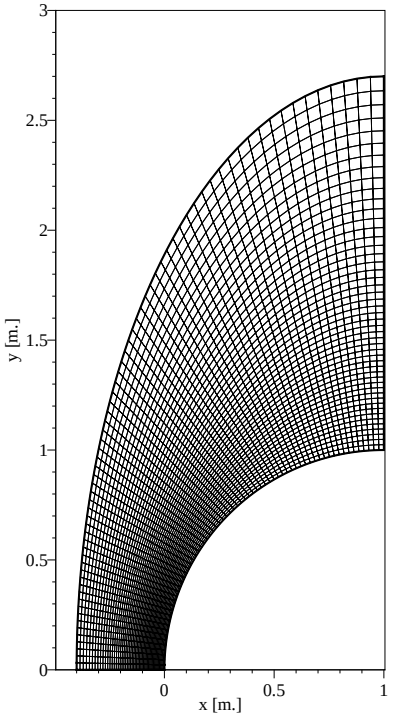

Fig. 4. Blunt body. Geometry and implemented mesh.

Int. J. Comput. Methods Downloaded from www.worldscientific.com
by NANYANG TECHNOLOGICAL UNIVERSITY on 08/06/16. For personal use only.

Table 2. Blunt body problem. Free stream conditions.

Test	ρ (kg/m^3)	p (Pa)	T (K)	V (km/sec)
1	8.8035×10^{-2}	5474.89	216.65	4.426
2	3.85×10^{-3}	277.52	2751.05	7.9408

equilibrium conditions. The blunt body corresponds to a cylinder of 1 m of radius and the physical domain of interest is discretized through a mesh, which has 70 and 35 nodes in tangential and radial directions, respectively (Fig. 4). Two free-stream conditions, which are described in Table 2, were considered. Boundary conditions on the symmetry line are implemented through first-order extrapolation values of density, internal energy and tangential velocity, while a zero normal velocity is imposed. Free-stream conditions are imposed at the supersonic inlet, while at the outlet, supersonic values obtained by first-order extrapolation are used. At the solid boundary, the tangential velocity is obtained by first-order extrapolation and the density is obtained by second-order extrapolation. Free-stream values are imposed

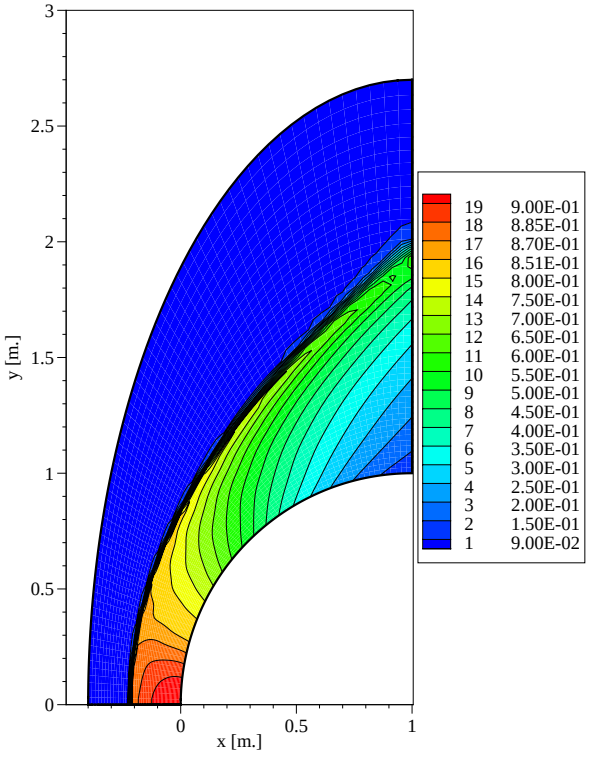

Fig. 5. Blunt body. Test 1. Density contour lines $\left(\frac{kg}{m^3}\right)$.

Int. J. Comput. Methods Downloaded from www.worldscientific.com
by NANYANG TECHNOLOGICAL UNIVERSITY on 08/06/16. For personal use only.

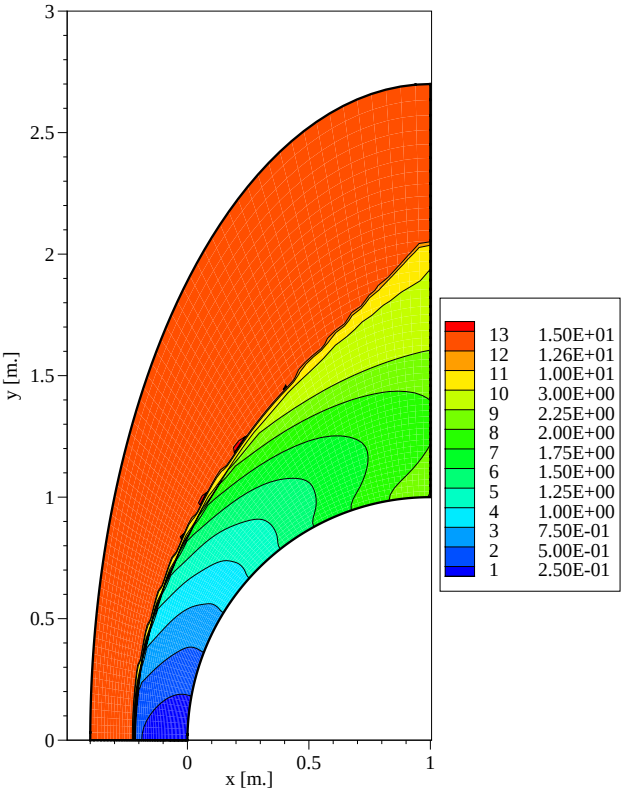

Fig. 6. Blunt body problem. Test 1. Mach contour lines.

as initial condition for the whole model domain. Time integration is carried out by means of the same Runge–Kutta explicit method used in unsteady flows. The parameter ϵ (Eq. (14)) is chosen equal to the spectral radius of the Jacobian matrix of the flux multiplied by a constant in agreement with the entropy fix proposed by [Yee (1986)] with the aim of avoiding convergence to unphysical solutions in blunt bodies hypersonic computations.

In Figs. 5 and 6, the numerical results of density and Mach number distribution respectively obtained for Test 1 with the HYMM scheme are shown. For the conditions of Test 2, Figs. 7 and 8 show the results of density and Mach distribution respectively obtained employing the HYAD scheme. It is possible to note that, both variants of Harten–Yee scheme provide similar results regarding accuracy in shock wave capturing along the stagnation line. However, in those regions of the model domain, where the mesh is not sufficiently well aligned with the shock wave, appears distortions in the shock wave capture, showing the dependence of the scheme on the mesh orientation. To evaluate the chemical behavior, the results obtained of the distribution of N_2 and O_2 employing the HYAD scheme for Test 2 are shown in Figs. 9 and 10, respectively.

Int. J. Comput. Methods Downloaded from www.worldscientific.com
by NANYANG TECHNOLOGICAL UNIVERSITY on 08/06/16. For personal use only.

Int. J. Comput. Methods Downloaded from www.worldscientific.com
by NANYANG TECHNOLOGICAL UNIVERSITY on 08/06/16. For personal use only.

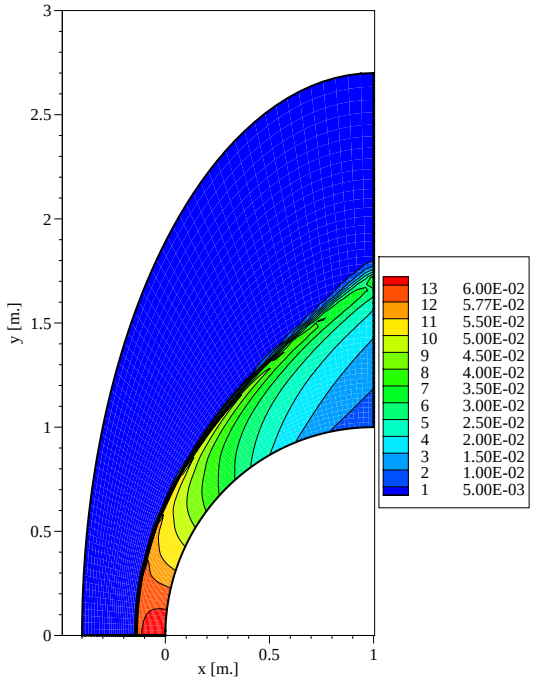

Fig. 7. Blunt body. Test 2. Density contour lines $\left(\frac{kg}{m^3}\right)$.

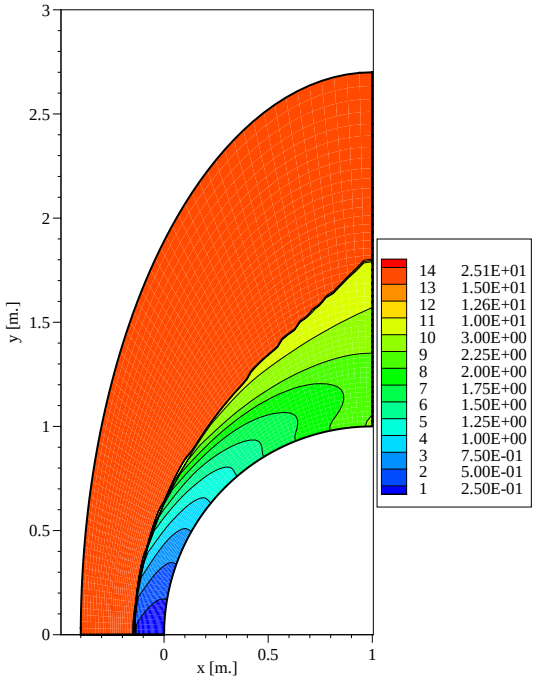

Fig. 8. Blunt body. Test 2. Mach contour lines.

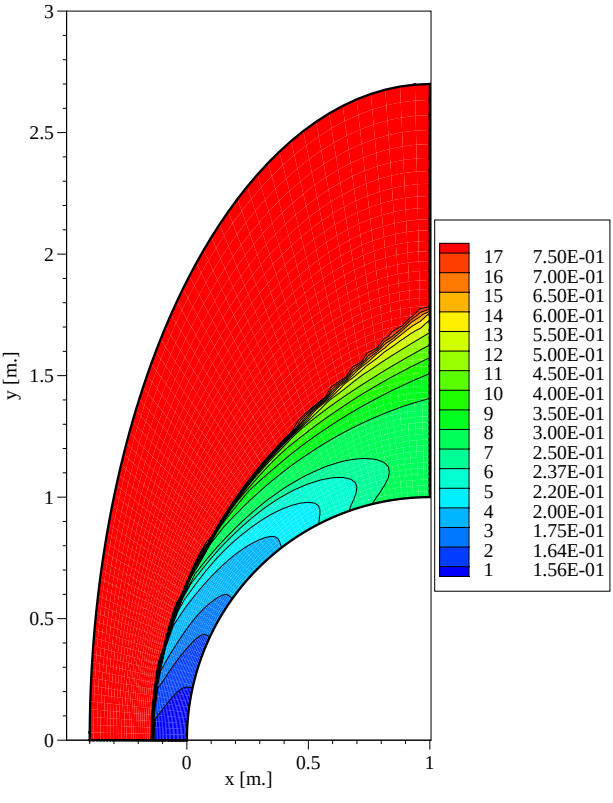

Fig. 9. Blunt body. Test 2. Distribution of N_2.

In Fig. 11, the temperature solution along the symmetry line is shown. In this plot, the results obtained through the three Harten–Yee scheme variants here implemented, HYAD, HYMM and HYNAD, are compared. Note that the capture of the normal shock wave is obtained in one cell width in all cases. The comparison between the temperature solution obtained with the HYAD scheme after the shock, and the exact solution obtained by solving the Rankine–Hugoniot conditions gives an error of approximately 0.1%. To evaluate and compare the steady-state convergence properties, the L_2-norm of the density residual evolution, considering both chemical equilibrium and calorically perfect gas, are shown in Fig. 12. The HYMM scheme provides the best convergence properties in comparison to the HYAD and HYNAD schemes, as is expected due to the discontinous nature of the *superbee* limiter function [Zheng and Lee (1998)]. Regarding this issue, although the adaptive technique HYAD has been able to achieve practically machine-zero convergence in the calorically perfect gas case, it has not improved the convergence properties of the nonadaptive technique HYNAD, when chemical equilibrium was considered. It was noted in numerical experiments, that when the *superbee* limiter

Int. J. Comput. Methods Downloaded from www.worldscientific.com
by NANYANG TECHNOLOGICAL UNIVERSITY on 08/06/16. For personal use only.

Int. J. Comput. Methods Downloaded from www.worldscientific.com
by NANYANG TECHNOLOGICAL UNIVERSITY on 08/06/16. For personal use only.

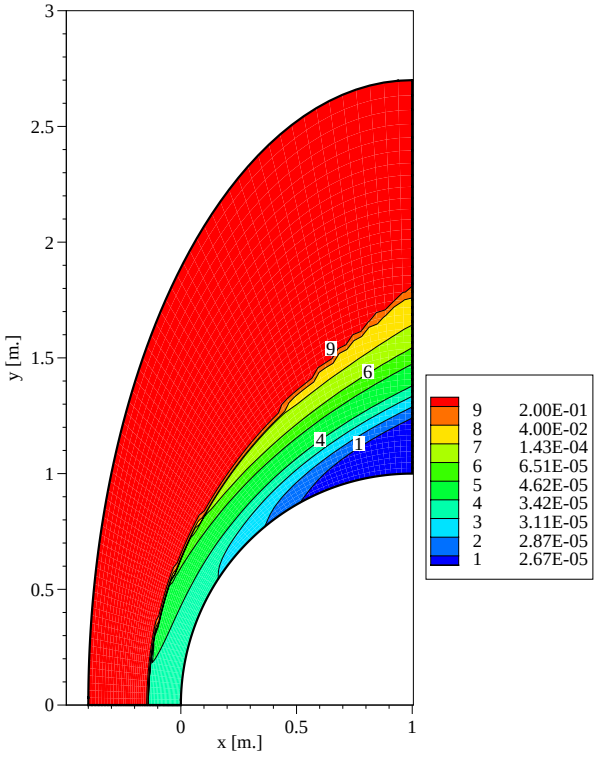

Fig. 10. Blunt body. Test 2. Distribution of O_2.

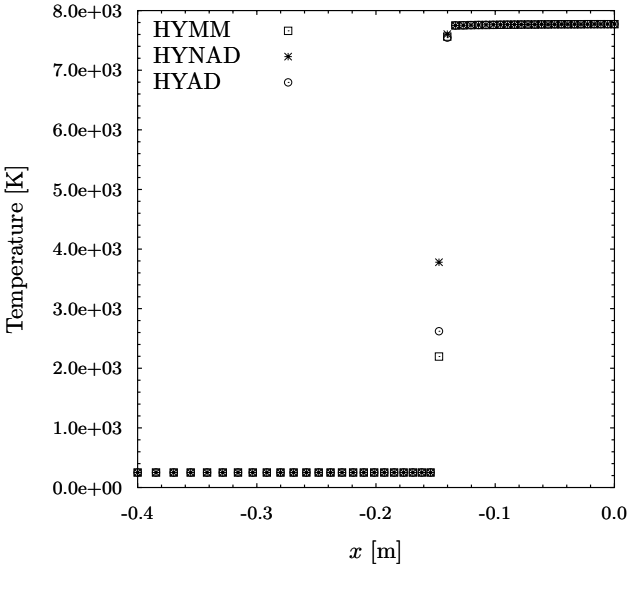

Fig. 11. Blunt body. Test 2. Temperature solution on the symmetry line.

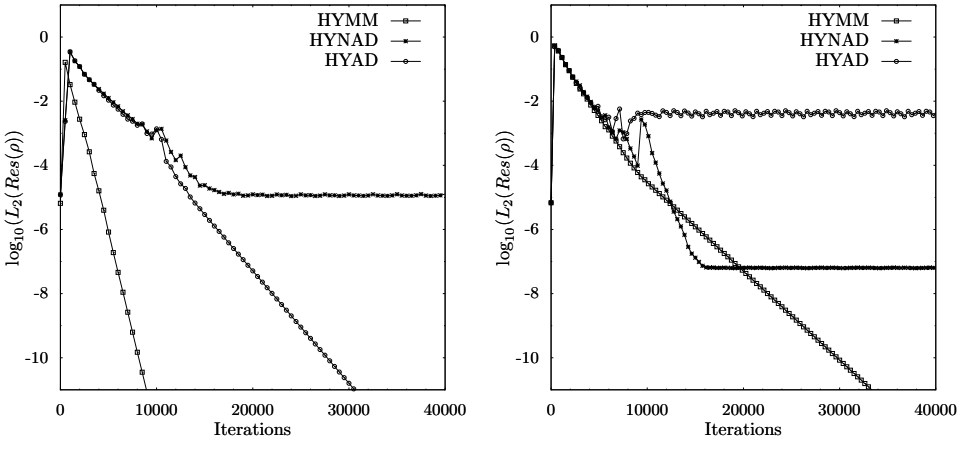

Fig. 12. Blunt body. Test 2. Steady-state solution convergence curves. (a) Calorically perfect gas and (b) Chemical equilibrium gas.

function is employed, local numerical oscillations appears close to the intersection between the sonic line and the shock wave, which prevents the convergence of the solution.

5. Conclusions

Three different variations of the finite difference Harten–Yee TVD scheme for the numerical solution of 2D, time-dependent and steady-state Euler equations have been implemented and tested. Depending on how they use the *minmod* and *superbee* limiter functions, these variations have been called HYMM, HYNAD and HYAD. Of particular interest was the extension of the adaptive technique (HYAD) proposed in [Falcinelli *et al.* (2008); Elaskar *et al.* (2009); Saldia *et al.* (2015)], when two-dimensional supersonic and hypersonic flows in chemical equilibrium are considered. For unsteady flows, numerical solutions of three different Riemann problems with cylindrical symmetry, specifically designed to validate numerical schemes for gas dynamics with chemical equilibrium effects have been presented. In these tests, both the HYAD and HYNAD schemes improve significantly the accuracy of contact discontinuity resolution in comparison to the classical HYMM scheme, while maintaining similar properties in shock wave capturing; also, it was found that the proposed adaptive technique (HYAD) reduced the oscillations that appears at the contact wave, when the *superbee* limiter function is employed (HYNAD). To study the behavior of the numerical schemes in steady-state flow simulations, solutions of the hypersonic flow over a blunt body have also been presented. Results obtained using the proposed adaptive technique are not significantly differenct with results computed using other previously well-tested variants of the Harten–Yee scheme.

Int. J. Comput. Methods Downloaded from www.worldscientific.com
by NANYANG TECHNOLOGICAL UNIVERSITY on 08/06/16. For personal use only.

However, it was noted that the use of the *superbee* limiter function reduces and also prevents the convergence to the steady-state solution.

Acknowledgments

This research was supported by CONICET, National University of Córdoba, MinCyT of Córdoba, Argentina.

References

Elaskar, S., Falcinelli, O., Tamagno, J. and Salda, J. [2009] "Further applications of scheme for reducing numerical viscosity: 3D hypersonic flow," *J. Phys. Conf. Series* **166**, 111–127.

Falcinelli, O., Elaskar, S. and Tamagno, J. [2008] "Reducing the numerical viscosity in nonstructured three-dimensional finite volume computations," *J. Spacecr. Rocket* **45**, 506–509.

Gordon, S. and McBride, J. B. [1994] "Computer program for calculation of complex chemical equilibrium compositions and applications," Part I : Analysis. NASA RP-1311.

Gottlieb, S. and Shu, C. [1998] "Total variation diminishing Runge–Kutta schemes," *Math. Comput.* **67**, 73–85.

Harten, A. [1983a] "On a class of high resolution total-variation-stable finite-difference schemes," *J. Comput. Phys.* **49**, 357–393.

Harten, A. and Hyman, J. M. [1983b] "Self adjusting grid methods for one-dimensional hyperbolic conservation laws," *J. Comput. Phys.* **50**, 235–269.

Leveque, R. [2004] *Finite Volume Methods for Hyperbolic Problems* (Cambridge University Press, Cambridge).

Montagné, J. L., Yee, H. C. and Vinokur, M. [1989] "Comparative study of high-resolution shock-capturing schemes for a real gas," *AIAA J.* **27**, 1332–1346.

Roe, P. L. [1986] "Characteristic-based schemes for the Euler equations," *Ann. Rev. Fluid Mech.* **18**, 337–365.

Saldía, J. [2012] "Simulación numérica de flujos de alta entalpía no viscosos considerando gas en equilibrio termodinámico. Master Thesis in Aerospace Engineering, Universidad Nacional de Córdoba", Argentina.

Saldia, J., Elaskar, S. and Tamagno, J. [2015] "A scheme for inviscid compressible flow, considering a gas in thermo-chemical equilibrium," *Int. J. Comp. Meth.* **12**(3), 1550015.

Tamagno, J., Elaskar, S. and Ríos, G. [2003] "Numerical simulation of time-dependent reacting flows in pulse facilities," *App Numer. Math.* **47**, 515–530.

Tannehill, J. and Mugge, P. [1974] "Improved curve fits for the thermodynamic properties of equilibrium air suitable for numerical computation using time dependent or shock-capturing methods," NASA, CR-2470. NASA.

Toro, E. [2009] *Riemann Solvers and Numerical Methods for Fluid Dynamics* (Springer, Berlin).

Vinokur, M. [1989] "An analysis of finite-difference and finite-volume formulations of conservation laws," *J. Comput. Phys.* **81**, 1–52.

Vinokur, M. and Montagné, J. L. [1990] "Generalized flux-vector splitting and Roe average for an equilibrium real gas," *J. Comput. Phys.* **89**, 276–300.

Whitham, G. [1974] Linear and Nonlinear Waves (John Wiley & Sons, New York).

Yee, H. C. [1986] "Numerical experiments with a symmetric high-resolution shock-capturing scheme," NASA TM 88325.

Int. J. Comput. Methods Downloaded from www.worldscientific.com
by NANYANG TECHNOLOGICAL UNIVERSITY on 08/06/16. For personal use only.

Yee, H. C. [1987] "Upwind and symmeric shock-capturing schemes," NASA TM 89464.
Yee, H. C. [1987] "Construction of explicit and implicit symmetric TVD schemes and their applications," *J. Comput. Phys.* **68**, 151–179.
Yee, H. C. [1989] "A class of high-resolution explicit and implicit shock-capturing methods," NASA TM 101088.
Zheng, B. and Lee, C. H. [1998] "The effects of limiters on high resolution computations of hypersonic flows over bodies with complex shapes," *Comm. Nonlinear Sci. Numer. Simul.* **3**(2), 82–87.

Int. J. Comput. Methods Downloaded from www.worldscientific.com
by NANYANG TECHNOLOGICAL UNIVERSITY on 08/06/16. For personal use only.